

10.1 INTRODUCTION

10.1.1 IMPORTANCE OF RISK-BASED SYSTEM ANALYSIS

With the worldwide transition toward low-carbon and sustainable energy utilization in recent years, the share of renewable generations is increasing rapidly in electricity systems. Till the end of 2018, the renewable generation (including hydro, wind, solar, biofuels, waste, geothermal, and tide) had reached 6879 TWh, an increase of 21.23% compared with 2015 [1]. In over 20 countries, the share of renewable generation exceeds 50%. A roadmap to complete renewable electricity in Europe and North Africa was proposed in [2]. In Denmark, the total wind generation equaled 47% of its electricity consumption in 2019, which continues to grow in recent years [3]. The US National Renewable Energy Laboratory proposed a blueprint that aims to realize 80% renewable electricity generation in 2050 [4]. China proposed carbon neutrality and peak carbon dioxide emission schemes, and focused on renewable generations as one of the solutions.

However, due to the fluctuation, intermittency, and unpredictability of the renewable generations, it also brings potential risks to the reliable and secure operation of electricity systems. In Denmark, it was reported that more than half of the power system's imbalanced situation was caused by the fluctuation of wind, and this kind of circumstances will occur more frequently in the future [5]. The random failure of the wind turbine itself may also become an important factor. In 2019, the simultaneous failures of Hornsea offshore windfarm and Little Barford gas-fired units (GFU) led to the blackout in the UK [6]. Therefore, it is important to study the system risks under the high penetration of wind.

10.1.2 MODELING OF THE UNCERTAINTIES OF WIND

In order to analyze the system's risks under the large penetration of wind, the prerequisite is the modeling of wind uncertainties. The prediction method of wind speed is categorized according to different standards, as illustrated in Figure 10.1. By timescale, it could be categorized into long term, medium term, short term, and ultra-short term. According to the different mathematical methods, it can be divided into mechanism- and data-driven approaches. According to different spatial scales, the prediction can be targeted on one single wind turbine, or a windfarm, or a cluster of adjacent windfarms. According to the output results, it can also be divided into point-by-point and probabilistic predictions.

FIGURE 10.1 Systematic interpretation of wind prediction methods.

The prediction of wind speed has been extensively studied in previous studies. A joint particle swarm optimization and gray method was used in the wind forecast in [7] to improve the accuracy. A pattern-based forecast method was proposed in [8] based on the unified key component evaluation. A multitime step-based operational wind generation forecast method was proposed in [9].

Besides the fluctuations in wind speed, the uncertainty of wind generation also comes from the random failure and repair of wind turbines. These two factors should be considered together. A reliability model of a windfarm was proposed in [10], considering both wind fluctuations and forced outages of wind turbines. The reliability of windfarm was studied in [11], which uses multistate Markov and cross-correlation function to represent the fluctuation of wind in several locations.

10.1.3 HANDLING THE UNCERTAINTIES OF RENEWABLE ENERGIES IN THE OPERATION OF POWER SYSTEMS

Many research papers have incorporated the uncertainties of renewable energies in the economic dispatch, scheduling, or planning of electricity systems. A comprehensive method for the probabilistic electric power flow was proposed in [12] to assess the fluctuation from photovoltaic generations on the electricity system operation. The simplified day-ahead scheduling method was proposed in [13] for wind generating units. A new scheduling method for generating units was established in [14] for promoting the reliability of electricity systems under high wind penetration. A risk-oriented stochastic optimization model for the capacity market was developed in [15] to minimize the maximum regret with renewable energies, and a practical case in China was investigated. Reliability-based expansion planning of electricity systems with renewable generations was conducted in [16] for lowering carbon emission.

On the other hand, a new rising technology, power-to-gas (P2G), offers a promising solution to the promotion the utilization of renewable energies. It can convert surplus electric generation from renewable generators into hydrogen or synthetic natural gas. By this means, the electricity can be indirectly stored for later use, thus preventing the waste [17]. Though the gas network does not require a precisely balanced supply and demand, excessive injection of gas into the gas network could still cause pressure fluctuations, threatening its secure operation. Under this new circumstance, the support from the gas system on renewable energy utilization and its influence on operational risks of electricity systems is worth studying. Some quantitative studies have been conducted to assess economic influence of P2Gs on the electricity systems and gas networks in the operation [18,19]. However, the impacts on system risk have not been studied yet, especially in terms of spatial and temporal risks.

10.1.4 EVALUATION OF SYSTEM OVER-LIMIT RISK INDICES

The risk evaluation of electricity systems with large penetration of renewable energies has been extensively studied in previous researches. Both long- and medium-term reliability indices were assessed in [20,21] using universal generating function techniques, respectively, with a large share of wind generation. The impacts of different wind power forecasting techniques on the risk evaluation of electricity distribution

networks were evaluated in [22]. The risk of unit commitment in wind integrated electricity systems was assessed in [23].

However, the studies described above focused on analyzing the risk in the long term over the whole system, while not considering the short-term and location-varying risks in the operational phase. The powers of renewable generations, such as wind and solar, vary in time and location [24]. For example, the photovoltaic generation is highly correlated with the light intensity, which is different throughout the day. The resource endowment of wind generation also varies from coastal mountain areas. This will result in different power flow patterns in the transmission system at different time points and further affect the risk in electricity systems [25]. Therefore, spatial-temporal risk analysis is urgently required.

The temporal risk, also known as short-term or operational reliability, has been previously studied in electricity systems. Reference [26] introduced the basic concept of operational reliability. It has been demonstrated as valuable information in risk-based scheduling, load shedding devising, and other decision-making processes. The short-term risk indices, which reflect the dynamic security of renewable generations, were proposed in [27]. The spatial risk is usually specified in nodal scales in the electricity system risk assessment. It helps nodal customers to estimate the reliability and quality of their electricity supply. The correlations between nodal energy price and nodal reliability indices were studied in [28]. The nodal reliability impact from electric vehicles on electricity systems was investigated in [29]. However, few studies have evaluated the spatial and temporal risks jointly or studied the impact of renewable generations on the electricity system risks in these two dimensions.

10.1.5 CONTRIBUTION OF THIS CHAPTER

To bridge the research gaps, this chapter proposes a spatial-temporal risk assessment approach in electricity systems under large penetrations of renewable generations. The contributions of the chapter are as follows:

1. The temporal and spatial reliability of the windfarm is modeled. Both spatial and temporal correlations in the wind speed prediction and the impact of wind turbine failures are jointly considered. Moreover, the multistate reliability models of coupling components, i.e., GFU and P2G, are modeled considering the interdependency between the electricity and gas systems.
2. An optimal control framework of the electricity system under the uncertainty of wind and integration of gas systems is proposed. To avoid the potential risks on the gas system operation by the gas injection of P2Gs, the constraints imposed by gas flow dynamics are incorporated in the optimal control framework.
3. The risk indices are extended in both time and space dimensions. To this end, the impact of renewables on the electricity system operation at different locations can be quantified. Furthermore, to reduce the computation burdens, the discretized partial derivative equations (PDEs) of gas flow dynamics are further relaxed into second-order cone (SOC) constraints, so that the off-the-shelf solvers can be applied more efficiently.

10.2 TEMPORAL AND SPATIAL MODELING OF UNCERTAINTIES

To study the risks to the electricity system during operation, the stochastic process of the available generating capacity of components, including the windfarm, GFU, P2G, and other traditional fossil generating units (TFU), should be modeled. Therefore, the temporal and spatial reliability of multiple windfarms is modeled, and the reliability models of GFUs and P2Gs are established.

10.2.1 TEMPORAL AND SPATIAL RELIABILITY MODEL OF WINDFARMS

The reliability of the windfarm is indicated by its available capacity to generate electricity [30]. It is related to two major factors, wind velocity and state of wind turbines. Wind velocity essentially depends on the weather system. It not only evolves in time, but is also correlated among different locations. Therefore, the precision will be significantly improved if we forecast the wind speed in both time and space dimensions.

In the operational phase, the Markov process is commonly adopted to approximate the chronological wind speed at a single location [5,21]. To establish the Markov process, the wind speed is first clustered into a finite set of states [31]. The number of states is flexible, depending on the accuracy requirement. Assume that wind speeds are the same for different wind turbines at the same windfarm. Generally, denote the number of states as NH_j^w at the windfarm j . During the operation, the wind speed takes random values from $\{v_j^1, v_j^2, \dots, v_j^{NH_j^w}\}$. Suppose the wind speed was at state h at $t = 0$. The time-varying probability of wind speed, $\Pr^h(t)$, at each state can be calculated by solving [21]:

$$\begin{cases} \frac{d\Pr^h(t)}{dt} = -\Pr^h(t) \sum_{h'=1}^{NH_j^w, h' \neq h} \lambda_{h,h'}^w + \sum_{h'=1}^{NH_j^w, h' \neq h} \Pr^{h'}(t) \lambda_{h',h}^w, h=1,2,4, \dots, NH_j^w \\ \Pr^1|_{t=0} = 0, 4, \dots, \Pr^{h_0}|_{t=0} = 1, 4, \dots = \Pr^{NH_j^w}|_{t=0} = 0 \end{cases} \quad (10.1)$$

where $\lambda_{h,h'}^w$ is the state transition rate from state h to h' .

To characterize the wind speed correlations in space, its concept is further extended into the temporal-spatial Markov process, as illustrated in Figure 10.2. The spatial Markov process was used in geostatistical, data processing, and image processing studies based on random field theories [32–35]. However, its applications in wind forecasting are still in their infancy. A spatial-temporal Markov process model was developed in [36] for ultra-short-term wind speed forecasting. This technique was further applied in the operational forecasting of renewable generation in [37]. To quantify the temporal and spatial effects of wind generation on the electricity system risks, it is extended to consider the random failures of wind turbines and then adopted in this chapter.

Given a dataset of wind speed, consider two windfarms j_1 and j_2 . The state transition probability from windfarm j_1 at state h_1 to the windfarm j_2 at state h_2 can be calculated as

$$\Pr_{j_1, j_2}^{h_1, h_2} = N_{j_1, j_2}^{h_1, h_2} / N_{j_1}^{h_1} \quad (10.2)$$

FIGURE 10.2 Temporal and spatial reliability model of windfarms.

where $N_{j_1}^{h_1}$ is the times when the state of wind speed at windfarm j_1 is h_1 . $N_{j_1, j_2}^{h_1, h_2}$ is the times when the state of wind speeds at windfarm j_1 and j_2 are h_1 and h_2 , respectively. When $j_1 = j_2$, it is defined as the self-transition probability as in the normal Markov process. Otherwise, when $j_1 \neq j_2$, it is defined as cross-transition probability, which describes the influence from the wind speed at other locations.

Repeat the above process until we obtain all the state transition probabilities. Then the state transition matrix between any two windfarms can be described as

$$\Pr_{j_1, j_2} = \begin{bmatrix} \Pr_{j_1, j_2}^{1,2} & \Pr_{j_1, j_2}^{1,2} & \dots & \Pr_{j_1, j_2}^{1, NH_{j_2}^w} \\ \Pr_{j_1, j_2}^{2,1} & \Pr_{j_1, j_2}^{2,2} & \dots & \Pr_{j_1, j_2}^{2, NH_{j_2}^w} \\ \dots & \dots & \dots & \dots \\ \Pr_{j_1, j_2}^{NH_{j_1}^w, 1} & \Pr_{j_1, j_2}^{NH_{j_1}^w, 2} & \dots & \Pr_{j_1, j_2}^{NH_{j_1}^w, NH_{j_2}^w} \end{bmatrix} \quad (10.3)$$

After formulating the state transition matrix for any pair of windfarms and giving the initial values of wind speed at all the locations, the future state of wind speed can be forecast utilizing time-sequential Monte Carlo simulation (TSMCS) [5]. However, the predicted wind speed at one location may have multiple possible values from other windfarms at various locations. We set them as reference values. The final predicted value of wind speed at windfarm j at period k , $\hat{v}_{j,k}$, is calculated by the weighted average [36]:

$$\hat{v}_{j,k} = \kappa_{1,j} v_{1,j,k} + \dots + \kappa_{j',j} v_{j',j,k} + \dots + \kappa_{NW,j} v_{NW,j,k}, \quad \sum_{j'=1}^{NW} \kappa_{j',j} = 1 \quad (10.4)$$

where $v_{j',j,k}$ is the wind speed at windfarm j predicted from windfarm j' at period k . NW is the number of windfarms. $\kappa_{j',j}$ is the weight coefficient from windfarm j' to windfarm j .

To calculate appropriate weight coefficients, the following optimization problem is formulated to minimize the prediction error in the given dataset:

$$\text{Min}_{\kappa_{f,j}} \sum_{k \in K} (v_{j,k} - \hat{v}_{j,k})^2 \quad (10.5)$$

where $v_{j,k}$ is the wind speed at windfarm j at period k in the given dataset. K is the set of periods.

According to the predicted wind speed, the available generating capacity of wind turbine l in windfarm j at period k , $G_{j,l,k}^{wt}$, can be calculated as [38]

$$G_{j,l,k}^{wt} = \begin{cases} 0 & , 0 \leq \hat{v}_{j,k} \leq v_{j,l}^{ci} \\ (A_{j,l} + B_{j,l} v_{j,k} + C_{j,l} \hat{v}_{j,k}^2) G_{j,l}^r & , v_{j,l}^{ci} \leq \hat{v}_{j,k} \leq v_{j,l}^r \\ P_{j,l}^r & , v_{j,l}^r \leq \hat{v}_{j,k} \leq v_{j,l}^{co} \\ 0 & , \hat{v}_{j,k} \geq v_{j,l}^{co} \end{cases} \quad (10.6)$$

where $v_{j,l}^{ci}$, $v_{j,l}^r$, and $v_{j,l}^{co}$ are the cut-in, rated, and cut-out wind speeds, respectively [39]. $A_{j,l}$, $B_{j,l}$, and $C_{j,l}$ are the parameters of the specific wind turbine. $G_{j,l}^r$ is the rated generating power of the wind turbine.

On the other hand, the operating state of the wind turbine is the other key factor determining its generating power. The reliability of a wind turbine can be described as the binary state. Thus, the available power generation capacity of windfarm j at period k , $G_{j,k}^w$, can be calculated as

$$G_{j,k}^w = \sum_{l=1}^{NL_j} I_{j,l}^w \times G_{j,l,k}^{wt} \quad (10.7)$$

where $I_{j,l}^w$ is a binary variable. $I_{j,l}^w = 1$ and 0 denote the perfect-functioning and complete-failure states, respectively. NL_j is the number of wind turbines at windfarm j .

10.2.2 OPERATIONAL RELIABILITY MODELS OF COUPLING COMPONENTS

GFU and P2G are the two main categories of coupling components between the electricity and gas systems. Different from the TFUs such as coal-fired units, the operational reliability of coupling components not only depends on their inherent failure and repair, but also relies on the just-in-time supply of the energy they consume, e.g., gas for GFUs and electricity for P2Gs.

1. Operational reliability model of GFUs

The operational reliability of GFU is represented using a multistate model. Its available electric generating capacity can be reduced partially or reduced to zero [40]. The number of states of the GFU j at bus i is

represented as $NH_{i,j}^{gfu}$. Thus, during the operational phase, the electric generating capacity of the GFU by random failure and repair takes values from

$$\left\{ G_{i,j}^{gfu,1}, 4, G_{i,j}^{gfu,h}, 4, G_{i,j}^{gfu,NH_{i,j}^g} \right\}.$$

The available generating capacity of a GFU also depends on the adequacy of the gas supply, which can be influenced by the status of natural gas networks. Thus, the actual electric generating capacity of GFU j at bus i , $DG_{i,j}^{gfu}$, can be calculated as

$$DG_{i,j}^{gfu} = \min \left\{ G_{i,j}^{gfu,h}, \left(-b_{i,j} + \sqrt{b_{i,j}^2 - 4a_{i,j}(c_{i,j} - HV \cdot w_{i,j}^{gfu})} \right) / (2a_{i,j}) \right\} \quad (10.8)$$

where $a_{i,j}$, $b_{i,j}$, and $c_{i,j}$ are the operating parameters of the GFU. HV is the calorific value of gas [41], and $w_{i,j}^{gfu}$ is the gas injection for the GFU during the operation.

2. Operational reliability model of P2Gs

The operational reliability of a P2G facility also depends on both its inherent state transition and the electricity supply. The P2G devices work in parallel in a practical P2G facility, and their operating conditions are fully independent [42]. The reliability of each P2G device is represented as the binary state. We assume that the parameters of the P2G devices, including failure and repair rates, and capacities are identical. During the operation, the gas production capacity $W_{i,j}^{p2g}$ of P2G module j at bus i takes random values from $\{0, W_{i,j}^{p2g}\}$. Therefore, the gas production capacity of the whole P2G facility is

$$W_i^{p2g} = \sum_{j=1}^{NP_i} I_{i,j}^{p2g} \times W_{i,j}^{p2g} \quad (10.9)$$

where $I_{i,j}^{p2g}$ is a binary variable. $I_{i,j}^{p2g} = 1$ and 0 denote the perfect-functioning and complete-failure states, respectively, and NP_i is the number of P2G modules at bus i .

Gas-producing capacities of P2Gs are also determined by the adequacy of the electricity at the bus where the P2G is located. The electricity supply may be affected by the status of the electricity system. Thus, the gas-producing capacity of the P2G facility can be evaluated as [18]

$$DW_i^{p2g} = \min \left\{ W_i^{p2g}, g_i^{p2g} / (\eta_i^{p2g} H_g) \right\} \quad (10.10)$$

where DW_i^{p2g} is the gas-producing capacity of the P2G at bus i . g_i^{p2g} is the electricity supply for the P2G at bus i during the operation. η_i^{p2g} is the efficiency of the P2G facility.

10.3 MODELING OF POWER SYSTEM AND UNCERTAINTY HANDLING APPROACH

During operation, failures of system components and fluctuation of wind power could occur, which might lead to the total power generation becoming inadequate for the demand. The generators or their reserve margins will be re-dispatched. In an even worse case, load curtailment might also be implemented to maintain a balanced operation. In particular, the natural gas system also participates in the re-dispatch process to back up the electricity system through GFUs, as well as to consume the surplus wind energy through P2Gs.

10.3.1 FORMULATION OF THE OPTIMAL CONTROL FRAMEWORK

The goal of the optimal dispatch is to optimize the generation and load curtailment costs. This economic loss of load curtailment can be implicitly quantified using customer damage functions [43]. Owing to the time-dependent characteristics of gas flow dynamics, the re-dispatch is optimized over a certain period, rather than a single time point in the traditional optimal dispatch. Therefore, the optimal re-dispatch is formulated as an optimal control problem:

$$\begin{aligned} \text{Min}_{g_{i,j,k}, g_{i,j,k}^{gfu}, w_{i,k}^{plg}, lc_{i,k}} J = & \sum_{k \in K} \left(\sum_{i \in GB} \left(\rho_{i,k}^g \left(\sum_{j \in NG_i^{gfu}} g_{i,j,k}^{gfu} / H_g - w_{i,k}^{plg} \right) \right) \right. \\ & \left. + \sum_{i \in EB} \left(\text{CDF}_i lc_{i,k} + \sum_{j \in NG_i} cst_{i,j}(g_{i,j,k}) \right) \right) \end{aligned} \quad (10.11)$$

Subject to (12)–(18), and constraints from the gas network:

$$G_{i,j}^{gfu, \min} \leq g_{i,j,k} \leq G_{i,j}^{gfu} \quad (10.12)$$

$$DG_{i,j}^{gfu, \min} \leq g_{i,j,k}^{gfu} \leq DG_{i,j}^{gfu} \quad (10.13)$$

$$0 \leq g_{i,j,k}^w \leq G_{i,j,k}^w \quad (10.14)$$

$$0 \leq w_{i,k}^{plg} \leq DW_i^{plg} \quad (10.15)$$

$$\sum_{j \in NG_i^{gfu}} g_{i,j,k}^{gfu} + \sum_{j \in NG_i} g_{i,j,k} + \sum_{j \in NW_i} g_{i,j,k}^w - g_{i,k}^{plg} - D_i^e - \sum_{j \in \Omega_i^e} f_{ij,k} = 0 \quad (10.16)$$

$$f_{ij,k} = (\theta_{i,k} - \theta_{j,k}) / X_{ij} \quad (10.17)$$

$$|f_{ij,k}| \leq f_{ij}^{\max} \quad (10.18)$$

where $w_{i,k}^{pg}$ and $g_{i,k}^{pg}$ are the gas production and electricity consumption, respectively, of the P2G j at bus i at period k , and $\rho_{i,k}^g$ is the gas production price. $g_{i,j,k}$ is the electric output of TFU j at period k . $cst_{i,j}$ is the generation cost function for TFU. GB and EB are the sets of gas and electricity buses. NG_i and $NG_i^{gf_u}$ are the sets of TFU and GFU at bus i , respectively. $G_{i,j}^{tf_u, \min}$ and $DG_{i,j}^{gf_u, \min}$ are the lower limits for the electric generations of TFU and GFU, respectively. $g_{i,j,k}^w$ is the electric generation of windfarm. NW_i is the number of windfarms at bus i . D_i^e is the electricity demand at bus i . Ω_i^e is the set of electricity branches linked to bus i . $f_{ij,k}$ is the electric flow from bus i to j . $\theta_{i,k}$ is the phase angle. X_{ij} is the reactance of the electricity branch ij . f_{ij}^{\max} is the capacity of electricity line ij . The constraints from the gas network are more complicated, which will be discussed in the next section.

10.3.2 DYNAMIC GAS NETWORK CONSTRAINTS

The idea of imposing constraints from the gas network is to limit the gas withdrawals and injections of GFUs and P2Gs, to ensure the secure operation of the gas network.

1. Reformulation of gas flow dynamic equations

Two PDEs, namely continuity and motion equations, govern the dynamics of gas flow in a pipeline. In a horizontal gas pipeline, the dissipative and isothermal gas flow is described by [44]:

$$\frac{B^2}{\rho_0 A} \frac{\partial q}{\partial x} + \frac{\partial p}{\partial t} = 0 \quad (10.19)$$

$$\frac{\partial p}{\partial x} + \frac{\rho_0}{A} \frac{\partial q}{\partial t} + \frac{2\rho_0^2 B^2}{F^2 DA^2} \frac{q|q|}{p} = 0 \quad (10.20)$$

where q and p are the quantity of gas flow and gas pressure, respectively. A is the cross-section area of the pipeline. B is the wave speed of natural gas. ρ_0 is the gas density at the standard temperature and pressure. D is the diameter. F is Fanning transmission coefficient.

The above PDEs for the pipeline ij can be discretized using the Wendroff formula [18]:

$$\frac{1}{B^2} (p_{m+1,k+1} + p_{m,k+1} - p_{m+1,k} - p_{m,k}) + \frac{\Delta t \rho_0}{\Delta x A} (q_{m+1,k+1} - q_{m,k+1} + q_{m+1,k} - q_{m,k}) = 0 \quad (10.21)$$

$$4 \left((p_{m+1,k+1} + p_{m+1,k})^2 - (p_{m,k+1} + p_{m,k})^2 \right) + \frac{\psi \rho_0 B^2 \Delta x}{F^2 DA^2} (q_{m+1,k+1} + q_{m+1,k} + q_{m,k+1} + q_{m,k})^2 = 0 \quad (10.22)$$

$$\text{sgn}(x) = \begin{cases} 1, & x \geq 0 \\ -1, & x < 0 \end{cases} \quad (10.23)$$

where Δx and Δt are the step sizes in length and time domains. m is the index of pipeline sections. ψ represents the direction of the gas flow, where $\psi = \text{sgn}(p_i - p_j)$. $\text{sgn}(x)$ is the sign function defined by (10.23).

Assume that the gas flow does not change direction during the operation [45]. Then, (10.22) can be further relaxed into SOC constraints:

$$\begin{aligned} & \left\| p_{m,k+1} + p_{m,k}, \sqrt{\frac{\rho_0^2 B^2}{F^2 DA^2}} \Delta x (q_{m+1,k+1} + q_{m+1,k} + q_{m,k+1} + q_{m,k}) \right\|_2 (1 + \psi) + \\ & \left\| p_{m+1,k+1} + p_{m+1,k}, \sqrt{\frac{\rho_0^2 B^2}{F^2 DA^2}} \Delta x (q_{m+1,k+1} + q_{m+1,k} + q_{m,k+1} + q_{m,k}) \right\|_2 (1 - \psi) \\ & \leq (1 + \psi)(p_{m+1,k+1} + p_{m+1,k}) + (1 - \psi)(p_{m,k+1} + p_{m,k}) \end{aligned} \quad (10.24)$$

3. Initial and boundary conditions

The initial and boundary conditions of the PDEs of the gas flow dynamics are specified in this subsection. The initial condition is given by the state variables of the electricity and gas systems in the normal state, where only the calculation of the gas flow in the steady-state is involved. The coordination of electricity and gas systems aims to minimize operating cost C_{IEGS} by controlling the generation schedule of TFUs and GFUs and the gas production schedule of gas sources:

$$\text{Min}_{w_i, g_{i,j}, g_{i,j}^{gfu}} C_{IEGS} = \sum_{i \in GB} \rho_i^g w_i + \sum_{i \in EB} \sum_{j \in NG_i} cst_{i,j}(g_{i,j}) \quad (10.25)$$

Subject to (10.26)–(10.29) and the constraints for electricity system (10.12)–(10.18):

$$w_i^{\min} \leq w_i \leq w_i^{\max} \quad (10.26)$$

$$w_i - D_i^g - \sum_{j \in NG_i^{gfu}} w_{i,j}^{gfu} + w_i^{ptg} - \sum_{j \in \Omega_i^g} q_{ij} = 0 \quad (10.27)$$

$$q_{ij} = C_{ij} \Gamma_{ij} \sqrt{p_i^2 - p_j^2} \quad (10.28)$$

$$|q_{ij}| \leq q_{ij}^{\max} \quad (10.29)$$

where w_i is the gas produced by the gas well at bus i . w_i^{\min} and w_i^{\max} are the minimum and maximum gas productions of the gas source. Ω_i^g represents the set of gas pipelines that are connected to bus i . q_{ij} denotes the gas flow from bus i to j . C_{ij} is a characteristic parameter of the pipeline, depending on the length, absolute rugosity, and some other properties. q_{ij}^{\max} denotes the maximum transmission capability in the gas pipeline ij .

After solving the optimization problem above, the values of w_i , $g_{i,j}$, and $g_{i,j}^{flu}$ can be obtained. During the intraday operation, the gas pressures in the pipeline segment m in period k , $p_{ij,m,k}$, should be controlled within the secure limits:

$$(1 - \gamma) p_{ij,m} \leq p_{ij,m,k} \leq (1 + \gamma) p_{ij,m} \quad (10.30)$$

where γ is the tolerance of gas pressure. The initial conditions for the gas pressure and gas flow are specified as

$$p_{ij,m,0} = \sqrt{p_i^2 - \Gamma_{ij} q_{ij}^2 (C_{ij}^2 L_{ij})^{-1} m \Delta x} \quad (10.31)$$

$$q_{ij,m,0} = q_{ij} \quad (10.32)$$

where L_{ij} is the length of the pipeline ij .

In the gas network, the boundary conditions among the pipelines are

$$p_{ij,0,k} = p_{ij_1,0,k} (\forall j_1 \in \Omega_i^g, \forall k) \quad (10.33)$$

$$p_{ij,0,k} = p_{j_2 i, M_{j_2}, k} (\forall j_2 \in \Omega_i^g, \forall k) \quad (10.34)$$

$$w_i - D_i^g + w_i^{ptg} - \sum_{j=1}^{NG_i^{flu}} w_{i,j}^{flu} + \sum_{j \in \Omega_i^g} q_{ji, M_{j_2}, k} - \sum_{j \in \Omega_i^g} q_{ij,0,k} = 0, \forall k \quad (10.35)$$

where M_{ij} is the number of pipeline segments in pipeline ij .

10.4 SYSTEM OVER-LIMIT RISK INDICES AND EVALUATION PROCEDURES

The spatial-temporal risk evaluation of the electricity system is the process of predicting risks for the system operator and nodal customers under a given system operating condition. TSMCS is used to sample the temporal and spatial wind speed, chronological random failure, and repair of generators and P2Gs during the operation and calculate the risk indices. The expected interruption of demand (EID) and risk of system overload (RSOL) of the electricity system are evaluated, as in (10.36) and (10.37) [23, 27]. It is worth mentioning that these two risk indices are extended to time-varying indices and are further specified into nodal scale, which provides better flexibility to reflect the impact of the temporal and spatial correlations of the renewables on the operational risks of the electricity system.

$$EID_i(t) = \left(\sum_{n=1}^{NS} \int_0^t I_{C_i}(\tau) d\tau \right) / NS \quad (10.36)$$

$$\text{RSOL}_i(t) = \left(\sum_{n=1}^{NS} \int_0^t \text{flag}(I_{C_i}(\tau)) d\tau \right) / NS \quad (10.37)$$

$$\text{flag}(x) = \begin{cases} 1, & x > 0 \\ 0, & x \leq 0 \end{cases} \quad (10.38)$$

where n and NS are the index and numbers of simulation times, respectively. $\text{flag}(x)$ is the flag function as defined in (10.38). The stopping criterion for the TSMCS is calculated by [46]

$$\max \left\{ \sqrt{\text{Var} \left(\sum_{i \in EB} \text{EID}_i(t) \right) / \sum_{i \in EB} \text{EID}_i(t)}, \sqrt{\text{Var} \left(\sum_{i \in EB} \text{RSOL}_i(t) \right) / \sum_{i \in EB} \text{RSOL}_i(t)} \right\} \leq \xi \quad (10.39)$$

where Var represents the variance function.

The temporal-spatial reliability evaluation procedure for the electricity system with renewable generation is presented with the following steps:

- Step 1:** Input wind speed data. Choose a random initial state for wind speed. Set the initial states of wind turbines, generators, and P2Gs to the perfect-functioning state.
- Step 2:** Calculate the initial operating condition of the gas system by solving the optimization problem in (10.12)–(10.18) and (10.25)–(10.29). Set the initial gas flow and pressure in the gas pipelines according to (10.31) and (10.32).
- Step 3:** Cluster the wind speed at each windfarm into NH_j^n states from the wind speed database. Calculate the state transition matrix between any pair of windfarms according to (10.2) and (10.3).
- Step 4:** Simulate the temporal and spatial wind speed according to (10.4). Compare the predicted value and the actual value in the wind speed database, and calculate the optimal weight coefficients by minimizing the prediction error, as in (10.5).
- Step 5:** Predict the wind speed at each windfarm with the given weight coefficients.
- Step 6:** Simulate the random failure and repair of wind turbines using TSMCS. Generate the available generating capacity sequence of windfarms according to (10.6) and (10.7).
- Step 7:** Simulate the random failures and repairs of GFUs, P2Gs, and TFUs according to section 10.2.2.
- Step 8:** Solve the optimal control of the electricity system considering the dynamics of gas flow, according to (10.11)–(10.18), (10.21), (10.24), (10.30), and (10.33)–(10.35), and then obtain the electric load curtailment.
- Step 9:** Calculate the temporal-spatial risk indices according to (10.36) and (10.37). Evaluate the stopping criterion for the TSMCS as in (10.39). If the criterion is satisfied, then output the risk indices as the final results. Otherwise, repeat the next simulation from Step 4.

10.5 INTERPRETATION OF PROBABILISTIC NUMERICAL ANALYSIS RESULTS

To verify the proposed temporal and spatial risk assessment technique, an IEEE 24-bus RTS [47] and the integration of Belgium natural gas system [48], as presented in Figure 10.3, is constructed in this section [49]. We replace the 400 MW nuclear generating unit at electric bus (EB) 18, a 100 MW unit at EB 7, and two 50 MW generators at EB 22 by windfarms of the same generating capacities. The model type and parameters of the wind turbine are set according to [30]. The oil steam generating units at EB 2, 13, 14, and 15 are replaced by the GFUs with the same capacity. Three P2Gs are installed at the gas bus (GB) 7, 10, and 16, and their capacities are set according to [49]. Other parameters including GFUs, P2Gs, gas prices, and heat value of gas are set according to [50]. The gas pressures are limited within 0.95–1.05 times of their values at the normal operating state. Numerical case studies were conducted on a Lenovo laptop with an 8565U CPU and 16GB RAM.

FIGURE 10.3 IEEE Reliability Test System with the integration of Belgium natural gas transmission system.

10.5.1 CASE 1: ANALYSIS OF WIND POWER, LOAD CURTAILMENT, AND GAS NETWORK

The wind speed data were acquired from the past ten years' historical data in Texas, the US, from the National Oceanic and Atmospheric Administration (NOAA). Four locations were compared, as in Figure 10.4. The probability density of the wind speeds in four areas presents similar patterns. This indicates that there may exist spatial correlations. We further cluster the wind speed into eight states for Monte Carlo simulation.

During simulation, one representative scenario is presented to elaborate on the effect of the large share of wind generation on the electricity system operation, and how the fluctuation of wind power influences the gas system through P2Gs.

As shown in Figure 10.5, the large share of wind generation could endanger the operation of electricity system operation, even if all other generating units function perfectly. At 3:00 and 7:00 before the 400 MW unit failure, there are small electric load curtailments of 0.25 and 0.89 MW, respectively. After the unit failure at 11:00, though the wind power is approximately the same during 12:00–16:00 as in 3:00–7:00, the electric load curtailment increases dramatically. The total electric

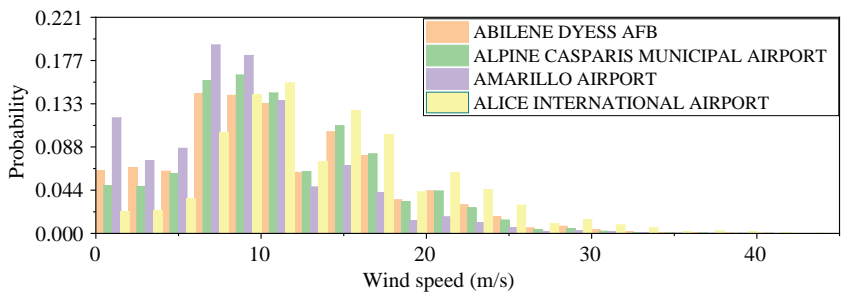


FIGURE 10.4 Histogram of wind speed data in Texas.

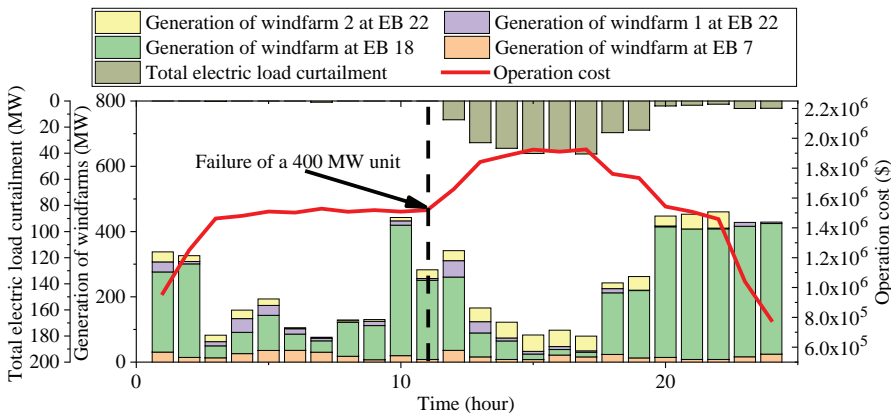


FIGURE 10.5 Wind generations, load curtailment, and operation cost in a representative scenario.

energy loss reaches 269 MWh. Due to this, the operation cost also increases. This indicates that with this level of wind penetration, the electricity system is vulnerable against possible failures of large generating units.

From the perspective of the gas system, as in Figure 10.6, we can observe that the gas system provides effective support to the electricity system. During the wind power’s peak period, P2Gs consumed surplus electricity and produced 0.13 Mm³ gas. While during the electricity generation shortage, the GFU raises its production by 24.16% to cover the electric load. Although the gas injection from P2Gs leads to slight fluctuations in the nodal gas pressures, they are still within a secure and controllable range.

10.5.2 CASE 2: TEMPORAL-SPATIAL RELIABILITY ANALYSIS

The temporal-spatial reliability indices are calculated in this case. EID and RSOL of the whole electricity system during the operational phase are shown in Figure 10.7. All components are preset in perfect-functioning states, so the system EID and RSOL are zero at the beginning. With the state transitions of wind speed and other generators, EID and RSOL increase to 2.58 MW and 0.023, respectively.

EID and RSOL during the operational phase are further specified to each EB, as presented in Figures 10.8 and 10.9, respectively. We can observe that EB 10, 9, and 5 have the highest EID and RSOL. Particularly for EB 10, its RSOL is significantly higher than that of other EBs, which indicates that those EBs are more likely to suffer load curtailment.

10.5.3 CASE 3: COMPARISON OF DIFFERENT WIND SPEED LEVELS

The endowment of wind power varies in different locations in the world. To draw a more generalized conclusion, this section conducts a sensitivity analysis, to explore the effect of different wind speed levels on temporal-spatial risks of the

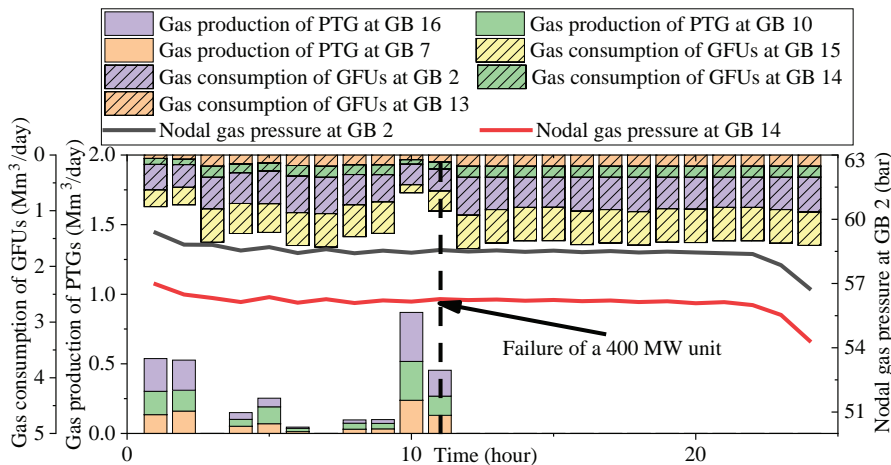


FIGURE 10.6 Gas production of P2Gs, gas consumption of GFUs, and nodal gas pressure in a representative scenario.

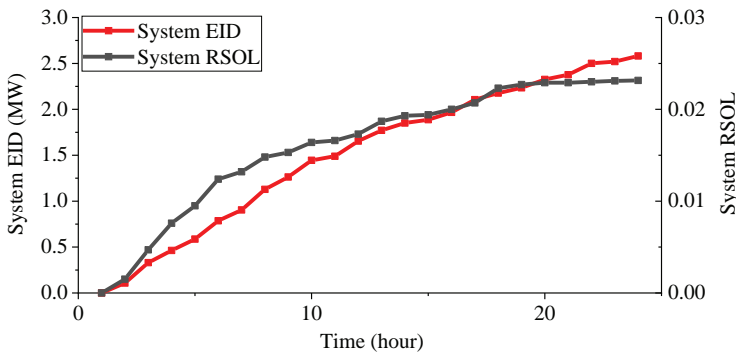


FIGURE 10.7 EID and RSOL of the electricity system.

electricity system. The probability distribution of wind speed is the same as in Case 1, while the expectation of the stochastic wind speed is different.

Figure 10.10 shows the variation of wind speed expectations with the system-level risk indices. With the increase in the expectation of wind speed, the system risk indices first decrease and then increase, which is due to the cut-out speed of the wind turbines. The lowest risks appear around 13.5–15 m/s.; above this speed zone, with

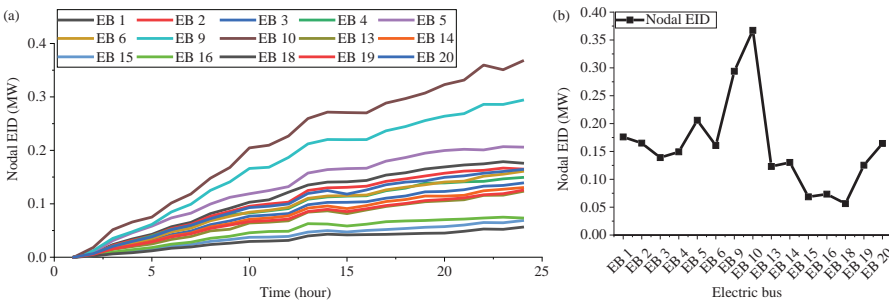


FIGURE 10.8 (a) Nodal EID during the operational phase. (b) Nodal EID at $t = 24$ h.

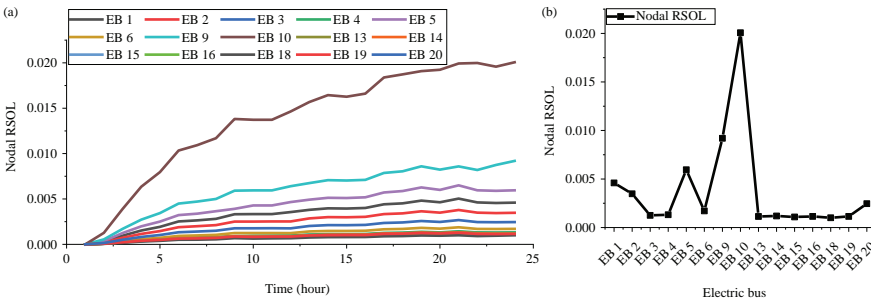


FIGURE 10.9 (a) Nodal RSOL during the operational phase. (b) Nodal RSOL at $t = 24$ h.

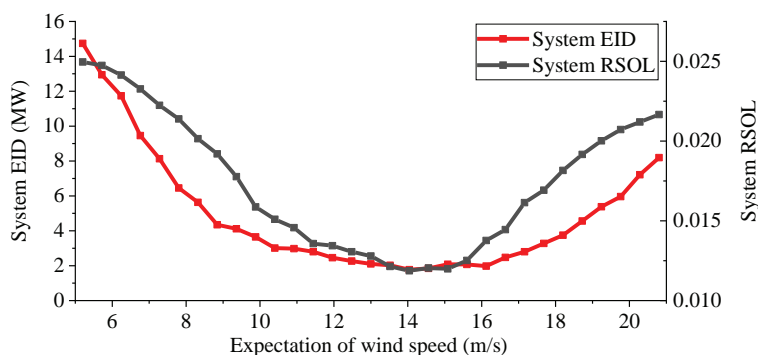


FIGURE 10.10 Sensitivity analysis of system risks with respect to the expectation of wind speed.

the increase of wind speed expectation, the wind speed will be more likely to exceed the cut-out speed, and the generation of windfarms will decrease. Thus, the electricity system becomes more likely to suffer a load curtailment.

10.6 CONCLUSIONS

The temporal-spatial risks of electricity systems under a large share of wind power have been evaluated in this chapter. Natural gas networks are integrated to the electricity system to promote the utilization of wind power. Numerical simulations indicate that the large share of renewable generations does have influences on the reliability of the electricity system. Its fluctuation, as well as intermittency, makes electricity systems more vulnerable against possible generating unit failures, e.g., the electric load curtailment even increased to 40.53 MW. On the other hand, the gas system provides effective support to the electricity system. During the wind generation's peak period, P2Gs consume electricity to produce 0.13 Mm³ gas, while during the electricity generation shortage, the GFU raises its production by 24.16% to satisfy the electric load. Furthermore, the temporal and spatial risk indices indicate that the risk of the system is increasing during the operation. EB 10 is most likely to suffer from load curtailment.

The conclusions strongly indicate the necessity of temporal and spatial risk evaluation when the electricity systems are highly penetrated with renewable energies. The risk assessment technique proposed in this chapter can be further developed and utilized in contingency management, day-ahead unit commitment, and other pertinent decision-making.

REFERENCES

1. IEA, "Data and statistics," International Energy Agency, 2020.
2. G. Schellekens, A. Battaglini, J. Lilliestam, et al., "100% renewable electricity: A road-map to 2050 for Europe and North Africa," 2010.
3. J. Gronholt-Pedersen, "Denmark sources record 47% of power from wind in 2019," A. Richardson and K. Donovan, eds., 2020.

4. T. Mai, D. Sandor, R. Wiser, et al., *Renewable electricity futures study. Executive summary*, National Renewable Energy Lab. (NREL), Golden, CO (United States), 2012.
5. Y. Ding, L. Cheng, Y. Zhang, et al., "Operational reliability evaluation of restructured power systems with wind power penetration utilizing reliability network equivalent and time-sequential simulation approaches," *Journal of Modern Power Systems and Clean Energy*, vol. 2, no. 4, pp. 329–340, Dec 2014.
6. J. Ambrose, "What are the questions raised by the UK's recent blackout?", 2019.
7. Y. Zhang, H. Sun, and Y. Guo, "Wind power prediction based on PSO-SVR and grey combination model," *IEEE Access*, vol. 7, pp. 136254–136267, 2019.
8. Q. Hu, P. Su, D. Yu, et al., "Pattern-based wind speed prediction based on generalized principal component analysis," *IEEE Transactions on Sustainable Energy*, vol. 5, no. 3, pp. 866–874, 2014.
9. N. Safari, C. Y. Chung, and G. C. D. Price, "Novel multi-step short-term wind power prediction framework based on chaotic time series analysis and singular spectrum analysis," *IEEE Transactions on Power Systems*, vol. 33, no. 1, pp. 590–601, 2018.
10. S. Sulaeman, M. Benidris, J. Mitra, et al., "A wind farm reliability model considering both wind variability and turbine forced outages," *IEEE Transactions on Sustainable Energy*, vol. 8, no. 2, pp. 629–637, 2017.
11. N. Nguyen, S. Almasabi, and J. Mitra, "Impact of correlation between wind speed and turbine availability on wind farm reliability," *IEEE Transactions on Industry Applications*, vol. 55, no. 3, pp. 2392–2400, 2019.
12. B. R. Prusty, and D. Jena, "A sensitivity matrix-based temperature-augmented probabilistic load flow study," *IEEE Transactions on Industry Applications*, vol. 53, no. 3, pp. 2506–2516, 2017.
13. R. Karki, S. Thapa, and R. Billinton, "A simplified risk-based method for short-term wind power commitment," *IEEE Transactions on Sustainable Energy*, vol. 3, no. 3, pp. 498–505, 2012.
14. M. Fan, K. Sun, D. Lane, et al., "A novel generation rescheduling algorithm to improve power system reliability with high renewable energy penetration," *IEEE Transactions on Power Systems*, vol. 33, no. 3, pp. 3349–3357, Feb 2018.
15. R. Lu, T. Ding, B. Qin, et al., "Reliability based min-max regret stochastic optimization model for capacity market with renewable energy and practice in China," *IEEE Transactions on Sustainable Energy*, vol. 10, no. 4, pp. 2065–2074, Oct 2019.
16. A. Moreira, D. Pozo, A. Street, et al., "Reliable renewable generation and transmission expansion planning: Co-optimizing system's resources for meeting renewable targets," *IEEE Transactions on Power Systems*, vol. 32, no. 4, pp. 3246–3257, Jul 2017.
17. J. Yang, N. Zhang, Y. Cheng, et al., "Modeling the operation mechanism of combined P2G and gas-fired plant with CO₂ recycling," *IEEE Transactions on Smart Grid*, vol. 10, no. 1, pp. 1111–1121, Jan 2019.
18. S. Clegg, and P. Mancarella, "Integrated modeling and assessment of the operational impact of power-to-gas (P2G) on electrical and gas transmission networks," *IEEE Transactions on Sustainable Energy*, vol. 6, no. 4, pp. 1234–1244, May 2015.
19. S. Chen, Z. Wei, G. Sun, et al., "Multi-linear probabilistic energy flow analysis of integrated electrical and natural-gas systems," *IEEE Transactions on Power Systems*, vol. 32, no. 3, pp. 1970–1979, May 2017.
20. Y. Ding, P. Wang, L. Goel, et al., "Long-term reserve expansion of power systems with high wind power penetration using universal generating function methods," *IEEE Transactions on Power Systems*, vol. 26, no. 2, pp. 766–774, Aug 2011.
21. Y. Ding, C. Singh, L. Goel, et al., "Short-term and medium-term reliability evaluation for power systems with high penetration of wind power," *IEEE Transactions on Sustainable Energy*, vol. 5, no. 3, pp. 896–906, Jul 2014.

22. M. Al-Muhaini, A. Bizrah, G. Heydt, et al., "Impact of wind speed modelling on the predictive reliability assessment of wind-based microgrids," *IET Renewable Power Generation*, vol. 13, no. 15, pp. 2947–2956, Nov 2019.
23. R. Billinton, B. Karki, R. Karki et al., "Unit Commitment Risk Analysis of Wind Integrated Power Systems," *IEEE Transactions on Power Systems*, vol. 24, no. 2, pp. 930–939, May 2009.
24. B. R. Prusty, and D. Jena, "An over-limit risk assessment of PV integrated power system using probabilistic load flow based on multi-time instant uncertainty modeling," *Renewable Energy*, vol. 116, pp. 367–383, 2018.
25. B. R. Prusty, and D. Jena, "A spatiotemporal probabilistic model-based temperature-augmented probabilistic load flow considering PV generations," *International Transactions on Electrical Energy Systems*, vol. 29, no. 5, pp. e2819, 2019.
26. S. Yuanzhang, C. Lin, Y. Xiaohui, et al., "Overview of power system operational reliability," In *2010 IEEE 11th International Conference on Probabilistic Methods Applied to Power Systems*, Singapore, 2010, pp. 166–171.
27. S. Datta, and V. Vittal, "Operational risk metric for dynamic security assessment of renewable generation," *IEEE Transactions on Power Systems*, vol. 32, no. 2, pp. 1389–1399, Mar 2017.
28. P. Wang, Y. Ding, and Y. Xiao, "Technique to evaluate nodal reliability indices and nodal prices of restructured power systems," *IEE Proceedings - Generation, Transmission and Distribution*, vol. 152, no. 3, pp. 390–396, May, 2005.
29. D. Tang, and P. Wang, "nodal impact assessment and alleviation of moving electric vehicle loads: from traffic flow to power flow," *IEEE Transactions on Power Systems*, vol. 31, no. 6, pp. 4231–4242, Feb, 2016.
30. A. S. Dobakhshari, and M. Fotuhi-Firuzabad, "A reliability model of large wind farms for power system adequacy studies," *IEEE Transactions on Energy Conversion*, vol. 24, no. 3, pp. 792–801, Sep 2009.
31. R. Karki, H. Po, and R. Billinton, "A simplified wind power generation model for reliability evaluation," *IEEE Transactions on Energy Conversion*, vol. 21, no. 2, pp. 533–540, Jun, 2006.
32. F. Melgani, and S. B. Serpico, "A Markov random field approach to spatio-temporal contextual image classification," *IEEE Transactions on Geoscience and Remote Sensing*, vol. 41, no. 11, pp. 2478–2487, Nov 2003.
33. R. Lowe, T. C. Bailey, D. B. Stephenson et al., "Spatio-temporal modelling of climate-sensitive disease risk: Towards an early warning system for dengue in Brazil," *Computers & Geosciences*, vol. 37, no. 3, pp. 371–381, Mar 2011.
34. W. J. M. G. Li, "Markov chain random fields for estimation of categorical variables," *Mathematical Geology*, vol. 39, no. 3, pp. 321–335, 2007.
35. Q. Yu, G. Medioni, and I. Cohen, "Multiple target tracking using spatio-temporal markov chain monte carlo data association," In *2007 IEEE Conference on Computer Vision and Pattern Recognition*, 2007, pp. 1–8.
36. Y. Zhao, L. Ye, Z. Wang, et al., "Spatio-temporal Markov chain model for very-short-term wind power forecasting," *The Journal of Engineering*, vol. 2019, no. 18, pp. 5018–5022, 2019.
37. M. He, L. Yang, J. Zhang, et al., "A spatio-temporal analysis approach for short-term forecast of wind farm generation," *IEEE Transactions on Power Systems*, vol. 29, no. 4, pp. 1611–1622, Jul 2014.
38. P. Giorsetto, and K. F. Utsurogi, "Development of a new procedure for reliability modeling of wind turbine generators," *IEEE Transactions on Power Apparatus and Systems*, vol. PAS-102, no. 1, pp. 134–143, Jan 1983.
39. Y. Sun, Z. Li, X. Yu, et al., "Research on ultra-short-term wind power prediction considering source relevance," *IEEE Access*, vol. 8, pp. 147703–147710, 2020.

40. M. Reshid, and M. Abd Majid, "A multi-state reliability model for a gas fueled cogenerated power plant," *Journal of Applied Science*, vol. 11, no. 11, pp. 1945–1951, 2011.
41. A. Seungwon, L. Qing, and T. W. Gedra, "Natural gas and electricity optimal power flow," In *2003 IEEE PES Transmission and Distribution Conference and Exposition*, Dallas, TX, USA, 2003, pp. 138–143.
42. G. Gahleitner, "Hydrogen from renewable electricity: An international review of power-to-gas pilot plants for stationary applications," *International Journal of Hydrogen Energy*, vol. 38, no. 5, pp. 2039–2061, Feb 2013.
43. G. Wacker, and R. Billinton, "Customer cost of electric service interruptions," *Proceedings of the IEEE*, vol. 77, no. 6, pp. 919–930, Jun 1989.
44. I. Cameron, "Using an excel-based model for steady-state and transient simulation," In *PSIG Annual Meeting*, St. Louis, Missouri, 1999, pp. 39.
45. Y. Zhou, C. Gu, H. Wu, et al., "An equivalent model of gas networks for dynamic analysis of gas-electricity systems," *IEEE Transactions on Power Systems*, vol. 32, no. 6, pp. 4255–4264, Nov 2017.
46. H. Jia, Y. Ding, Y. Song, et al., "Operating reliability evaluation of power systems considering flexible reserve provider in demand side," *IEEE Transactions on Smart Grid*, vol. 10, no. 3, pp. 3452–3464, May 2019.
47. C. Grigg, P. Wong, P. Albrecht, et al., "The IEEE reliability test system-1996. A report prepared by the reliability test system task force of the application of probability methods subcommittee," *IEEE Transactions on Power Systems*, vol. 14, no. 3, pp. 1010–1020, Aug 1999.
48. D. De Wolf, and Y. Smeers, "The gas transmission problem solved by an extension of the simplex algorithm," *Management Science*, vol. 46, no. 11, pp. 1454–1465, 2000.
49. W. Sheng, D. Yi, Y. Chengjin, et al., "Reliability evaluation of integrated electricity–gas system utilizing network equivalent and integrated optimal power flow techniques," *Journal of Modern Power Systems and Clean Energy*, vol. 7, pp. 1523–1535, Oct 2019.
50. C. Unsuhay, J. W. M. Lima, and A. C. Zambroni de Souza, "Modeling the integrated natural gas and electricity optimal power flow," in *2007 IEEE Power Engineering Society General Meeting*, Tampa, FL, USA, 2007, pp. 1–7.

